Bio-Based Materials in a Synthetic World: Activity and Longevity in Functional Films

Eric B. Williams[a], Melinda Wales[b], Steve McDaniel[b], and James W. Rawlins[a]
[a] The University of Southern Mississippi, USA
[b] Reactive Surfaces Ltd., USA

Traditionally, coatings systems were developed and engineered to optimally hide, beautify, and/or protect a substrate. Functionality is the most recent technology advancement to enhance the role of coatings designed and engineered to interact dynamically with users. The incorporation of natural functional materials such as enzymes and peptides into coatings yields functional films that offer novel possibilities in diverse applications. Once harvested, stabilized or mimicked, and then incorporated, coating surfaces have been shown to self-detoxify, self-clean, degrease, and self-sterilize by functional design. The novel biomaterials are generally non-persistent, non-toxic, and renewable for coatings utility and longevity.

Our research focus is on paving the way to understand "smart" functional additives. Using organophosphate hydrolase (OPH) biocatalyst with varying polymers and model challenge agents, sympathetic/antithetic relationships are being studied to gain depth of understanding and define the functional limits in varying environments in both activity and longevity. The data reported herein validate that the catalytic characteristics of an embedded biocatalyst are dramatically altered and improved by judiciously matching the polymer type with the biomaterial. The sorption of the reactants into the polymer coating and their correlation with OPH hydrolysis rates will be discussed. This study clarifies that proper pairing of polymer and bio-molecules result in stable, active, and diversely functional surfaces capable of maintaining full protective and decorative characteristics.

Introduction

Traditionally, protective and decorative coatings have provided function by acting as a barrier to the surface or by providing surface hiding properties. Intrinsic functionality is achieved through the judicious selection of additives, pigments and polymer, with the polymer or binder choice typically dominating the coating's overall performance. Embedding enzymes within polymeric films and coatings presents an opportunity to add active functionalities to these traditional materials. Enzyme behavior in aqueous solutions has been explored since the advent of biochemistry. It is well established that environmental conditions, such as ionic strength and pH, affect reaction rates of enzyme-catalyzed reactions. In the early 80s, the determination that enzymes were active in organic solvents [1] was remarkable not only because it challenged the commonly held view that enzymes cannot function in nonaqueous environments, but also opened up new possibilities for exploitation of biocatalyst properties, specifically in organic media. The identification of a "pH memory" effect was an important conceptual advance in understanding low water catalysis, and is attributed to the retention of a water shell on the enzyme surface, which was shown to be at the same pH as the aqueous solution from which the enzyme was extracted.[2] Since substrate/product diffusion into and out of the active site have to move through this water shell and into the organic phase, activity in organic solvents can be enhanced by tuning the polarity of the enzyme microenvironment and the organic phase to that of both the reactant and the product.[3]

Enzymes catalyze chemical reactions in natural systems by converting substrates (reactants) into products *via* an enzyme-substrate complex. The enzyme catalytic site (containing approximately ten amino acid residues) solvates the reactant(s) to form the enzyme-substrate complex. Subsequent dissociation of the enzyme-substrate complex forms product(s) and free enzyme upon successful

conversion. The conformation of the active site is similar to the conformation of the reactant's transition state that forms as the reaction proceeds from reactants to products (or vice versa). The progression from reactants to a transition state is favored by non-covalent stabilization within the active site via hydrogen bonding and/or electrostatic interactions. The binding energy between the enzyme active site and the bound intermediate molecule accounts for the loss of activation entropy as a consequence of reduced translational and rotational motions. Therefore, the three dimensional conformation of the enzyme active site is crucial to the binding conformation between the enzyme and the intermediate state of the reaction. Enzymes lower the activation energy proportional to the binding energy of the forward and reverse reactions. It must be noted that enzymes, like traditional chemical catalysts, do not shift/alter the equilibrium, but only the rate at which equilibrium is established. Consequently, in a closed system, enzymes decrease the reaction time required to establish equilibrium.[2]

Similar to low water/organic catalyst, the advent of enzyme immobilization significantly expanded the use of enzyme catalyst to a variety of applications, e. g., heterogeneous biocatalyst, selective adsorbent, controlled released protein drugs, analytical devices, and solid phase protein chemistry for insoluble enzymes.[4] Generally, enzyme immobilization confers additional stability to the biocatalyst by "freezing" in conformations that exist in solution prior to immobilization. Several immobilization approaches have been investigated including adsorption, covalent binding, entrapment, and membrane confinement.[5] Adsorption techniques entail enzyme attachment to the solid support by surface-to-surface interactions, such as electrostatic and hydrophobic. Immobilization by covalent attachment involves crosslinking the enzymes with solid functionalized supports and is particularly useful in applications where enzyme leakage is undesirable.[6] Enzyme entrapment in sol-gel is also a widely used method for enzyme immobilization.[7] The range of temperature and pH stability of enzymes can be highly improved by confining the enzyme to the sol portion of the support.[7] Much of the literature discussing enzyme-catalyzed reactions in "constricted" media comes from enzyme immobilization and polymer degradation research. Chemical parameters, such as enzyme/matrix and substrate/matrix interactions, can confer intrinsic polarity to each component that are summed up quantitatively as Hansen solubility parameter, and algebraically express the energy associated with the net attractive interaction in the form of logarithm of partition (log P) values.[8]

Physical parameters become prominent when the matrix imposes mass transfer limitations that affect enzyme-catalyzed reaction rates by lowering the diffusion rates of substrates and products. Novick and Dordick studied the impact of diffusional constraints by copolymerizing a vinyl functionalized α-chemotrypsin with a series of vinyl monomers. They determined that increasing the polymer matrix average mesh size by plasticization increased the rate of substrate diffusion and resulted in higher enzyme activity. In the same study, decreasing the crosslink density also translated in higher observed activity corroborating the concept that a larger mesh size supports higher rates of substrate diffusivity and leads to higher observed activity.[9] The correlation between substrate diffusivity and activity was further enlightened by Gross and coworkers, who demonstrated the influence of diffusional constraints on the rate of enzyme-catalyzed polymerizations by varying the length of a tortuous pathway for migration of substrate and polymer products.[10]

Biomolecules have been shown to retain their activity after incorporation in commercial coatings.[11] However, the effects of the polymer on biocatalyst activity are not well understood. Reactive surfaces represent a developmental frontier for coatings with unique properties as they contain isolated natural materials that retain their activity upon incorporation into a synthetic environment. Our research focus is to study, understand and develop systems using natural additives where enzymes and reactants are dispersed, embedded, and maintained within a continuous polymer phase either as solid films or aqueous dispersions. Thus, the polymer, enzymes, and reactants are blended to form a single macroscopic phase without negatively affecting enzyme activity. Upon shrewd selection and/or modification of the embedded biocatalyst, the factors that ultimately control the enzyme efficiency are the physical and chemical properties of the polymer.[12] Reactant and product diffusion rates can be correlated to polymer free volume in the absence of specific binding interactions, which is common when predicting transport phenomena within polymers.[13] The free volume theory is applicable to describe complex diffusion processes because it relies on measurable and readily available physical parameters.[13] On the other hand, chemical interactions of polymer units with other system components are best described by differences between their Hansen solubility parameters and summarized most simplistically as the old adage "like likes like". The integration of these various influences into a conceptual understanding, and

development of the methodology to monitor and assess the critical variables, will allow for a more complete understanding of the utility for functional coating systems and allow for moving products through development into a commercial product in the shortest time.

Materials, Methods, and Film Characterization

The polymer resins used to evaluate functional film activity in this study were Avanse® MV-100 emulsion, Joncryl® 74 dispersion, Eponol® 53-BH-35, a linear thermoplastic epoxy resin, and Hybridur® 570/580 polyurethane dispersion, which is a resin blend of Hybridur® 570 (72.2%) and Hybridur® 580 (27.8%). Avanse MV-100, an emulsion with a measured glass transition temperature (T_g) of 13.8 ℃, contains acrylic monomers that can crosslink auto-oxidatively, and is typically used for direct-to-metal coatings for industrial maintenance applications. Joncryl 74, an acrylic polymer with a measured T_g of -11.6 ℃, does not crosslink auto-oxidatively, and is typically used in overprint varnishes and inks. Hybridur 570/580, an acrylic–urethane hybrid polyurethane dispersion with a measured T_g of -33.1 ℃, is used as an adhesive, a general top coat, or plastic coating. Eponol 53-BH-35 is an ultra high molecular weight linear epoxy functional resin with a measured T_g of 90.5 ℃, contains approximately 90 bisphenol-A glycidyl ether repeat units, and is employed in adhesives, laminates, shop primers, and high performance finishes. T_g values were measured via differential scanning calorimetry using a Thermal Analysis TA Q2000 DSC and Universal Analysis 2000 software v4.5A. The T_g was calculated from the third thermal cycle of 10 ℃/min ramp from -20 ℃ to 120 ℃. The polymer types and characteristics above were chosen for optimum diversity in our initial investigations.

The biobased additive selected for these studies was OPDtox™ (Reactive Surfaces, Austin, TX), which contains the active Organophosphorus Hydrolase (OPH) enzyme within a natural material matrix, i.e., enzyme from the natural state without chemical modification or denaturing purification. The OPH enzyme is naturally specific for the hydrolytic cleavage of the phosphoric ester and thioester linkage in molecules. The reactants for these experiments include the chemical warfare agent simulants, paraoxon and/or demeton-S (to avoid confusion, reagents are termed substrates in biochemistry), and deionized, distilled water (DiH_2O). The organophosphate agent simulants contain a phosphoester bond between diethylphosphate and *p*-nitrophenol (paraoxon) and a phosphothioester bond between dimethylphosphate and ethanethiol (demeton-S), respectively. The simulants were obtained from Chem Services, PA, and used as supplied without further purification.

A Mettler Toledo ReactIR™ (iCIR10) was coupled to a temperature controlled Durasampler™ set to 25 ℃, and the resins were drawn across the detector diamond and heated stainless steel surfaced at 8 mils wet film thickness. The films were allowed to dry for at least 18 hours before initiating characterization protocols by the ICIR10 set to 182 scans per minute at one minute intervals. For neat challenge agents, 2.6 µg of undiluted paraoxon or demeton-S (as noted below) was applied to the film surface, covered to protect the air-surface interface, and monitored for three hours to determine paraoxon or demeton-S sorption at the film-substrate interface. The initial rate calculations for sorption based on the IR signature for the identified components using Mettler-Toledo iCIR v4.1.882 analysis software were plotted against $(time)^{1/2}$. To better understand the aqueous sorption rate in conjunction with the polymer affinity for paraoxon or demeton-S solvated in water, 40 µL of 15 mM aqueous challenge was applied to the dry film surface and monitored for sorption as described above. The rate of water sorption was plotted against the absorbance of paraoxon at 1530 to 1496 cm^{-1} (based on the independent absorbance of paraoxon from water and the polymer film in the aromatic stretching region for conjugated carbon double bonds). The rate of demeton-S sorption was plotted against the absorbance region of 1350 to 1250 cm^{-1} (selected for the phosphoryl absorbance bands on demeton-S).

Coatings containing the enzyme additive, termed biocatalyst enhanced coatings, were prepared by the addition of 0.2 g/mL aqueous OPH additive to the selected resins at 3% by weight of additive to total resin solids. OPH-containing solvent-based coatings were prepared by blending 3% dry OPH additive (on total resin solids) with Eponol in a FlackTek™ vortex mixer for 90 sec at 3000 rpm. Each coating was applied onto polypropylene sheets at 8 mils wet film thickness. The final coating thickness was measured with an ultrasonic micrometer by placing the free film on a nonferrous surface. The film thicknesses (reported as averaged for triplicate films measured in seven different locations) were determined to be Hybridur-Ctrl 48 ± 12 µm, Hybridur-OPH 46 ± 11.5 µm, Joncryl-Ctrl 41 ± 10.25 µm, Joncryl-OPH 41 ± 10.25 µm, Avanse-Ctrl 77 ± 19.25 µm, Avanse-OPH 73 ± 18.25 µm, Eponol-Ctrl 55 ± 13.75 µm, and Eponol-OPH 50 ± 12.5 µm.

To measure the water uptake in dried coatings, the free films were sectioned into triplicate 2 cm^2 samples and the initial mass of the film samples was recorded. The films were submerged in deionized water for 8 h and the mass change was recorded after wicking off excess water. The recorded mass increase upon water immersion in each polymer type was 10.7 ± 4.2 mg in Avanse MV-100 (146.7 %), 3.3 ± 0.7 mg in Joncryl 74 (47.3 %), 0.5 ± 0.1 mg in Hybridur 570/580 (7.1 %), and 0.4 ± 0.1 g in Eponol 53-BH-35 (8.4 %).

Each coating's hydrophilicity/hydrophobicity was characterized via water contact angles measured using a First Ten Ångstroms' FTÅ200 platform and analyzed by FTA32 v2.0 analysis software in triplicate using dried films drawn at 4 wet mils on aluminum panels. The recorded contact angles for each film was 47.99 ± 0.24°for Avanse MV-100, 84.21 ± 2.74°for Joncry l 74, 62.40 ± 1.52°for Hybridur 570/580, and 75.84 ± 2.21°for Eponol 53-BH-35.

The reactant sorption was correlated with the OPH additive (OPDtox) activity via UV/Vis spectroscopy. The enzymatic breakdown of paraoxon results in the formation of diethyl phosphate and *p*-nitrophenol. The *p*-nitrophenol ($Є_{405}$ = 17,000 M^{-1} cm^{-1}, pH 8.0) concentration was monitored spectroscopically as a function of catalysis. Demeton-S hydrolysis was monitored by coupling the reaction product ethanethiol to Ellman's reagent [5,5'-dithio-bis(2-nitrobenzoic acid) – DTNB]. Each reaction contained 60 mM DTNB ($Є_{405}$ = 13,600 M^{-1} cm^{-1}, pH 8.0) and was monitored at 405 nm spectroscopically as a function of catalysis. Films were extracted in uniform dimension using a hole-punch to yield 29.6 mm^2 samples before initiating neat paraoxon or demeton-S catalysis by applying 1.13 µg to one side of the sample and spreading it evenly to coat the entire surface. Triplicate samples were then quickly transferred to the inner wall of individual wells of a 96-well plate and held in place by nonbinding retainer rings to allow unimpeded light transmission by the film sample. 200 µL of 40 mM CHES, pH 9.1 reaction buffers, lacking paraoxon or demeton-S, was placed in each well and monitored continuously for 33 min to identify changes in absorbance at 405 nm. A saturated aqueous solution (1% paraoxon or demeton-S) was prepared 72 hours before use to ensure maximum solvation of paraoxon or demeton-S. To initiate kinetic characterization of the coating system using aqueous saturated reactants, 100 µL of 80 mM, pH 9.1 reaction buffer and 100 µL of 1% aqueous challenge agent were added to the sample well containing a 29.6 mm^2 film disk and monitored continuously for 33 min to observe changes in absorbance at 405 nm.

Results

Diffusion Response of Simulate Agents and Water Singularly and in Combination versus Polymer Type

Polymer selection was designed to compare a broad range of polymer types and properties for varying diffusion rates with the embedded OPH activity within solid film supports. Calculations of the diffusion coefficient as described by Talbot and Kitchener[14] were evaluated for changes at reduced times using the modified diffusion equation 2, where n represents $^{1/2}$ for Fickian sorption or 1 for non-Fickian sorption characteristics.[15-16]

$$\frac{A_t}{A_\infty} = 1 - \sum_{n=0}^{x} \left[\frac{8}{(2n+1)^2 \pi^2} \exp\left(\frac{-D(2n+1)^2 \pi^2 t}{4L^2} \right) \right] \quad \text{(Eq. 1)}$$

$$\frac{A_t}{A_\infty} = \frac{4}{L} \cdot \left(\frac{Dt}{\pi} \right)^n \quad \text{(Eq. 2)}$$

The sorption profile indicated that a near Fickian sorption characteristic of neat paraoxon occurred in Eponol (Figure 1) with a $T\text{-}T_g$ value of -65.5 ℃. The observed sorption profile of neat demeton-S into Eponol followed a characteristic Fickian profile (Figure 2). Compared to the diffusion of the water saturated paraoxon (Figure 3) or demeton-S (Figure 4), the sorption profile became non-Fickian for both challenge agents. Given that both challenge agents are solvated in water for the aqueous challenge, one might expect that if the water were the determinant sorption characteristic, then both aqueous profiles would be similar. However, while the sorption of solvated paraoxon into Eponol followed a sigmoidal pseudo-Fickian profile as described by Park[17] with a diffusion coefficient of 1.62 x 10^{-9} cm^2 s^{-1}, and the sorption of solvated demeton-S followed what may be described as a near Fickian sigmoidal process following the characteristics described by Bagley and Long[18] with a diffusion coefficient of2.25 x 10^{-10} cm^2

s^{-1}. The alteration of sorption profiles using water to carry the challenge agent into the coating resulted in independent sorption profiles based on the challenge agent solvated in the aqueous carrier. The data suggest the premise that polymer selection in functional coatings has controlling significance in sorption of the challenge agent for embedded solid phase catalysis.

The acrylic films, Avanse MV-100 and Joncryl-74, had a measured T-T_g of 11.2 ℃ and 36.6 ℃ respectively. Both acrylic films were in the rubbery region at the experimental conditions observed. The sorption profile for neat the challenge agents paraoxon (Figure 5) and demeton-S (Figure 6) into the Joncryl-74 films followed pseudo-Fickian sorption characteristics. The sorption profile of neat paraoxon into an Avanse MV-100 film was observed to be two-step non-Fickian (Figure 7); however, the sorption profile for demeton-S into an Avanse MV-100 film was two-step initial sorption and Fickian second step (Figure 8) as described using the characteristics defined by several authors.[18-21]

The aqueous saturated paraoxon challenge agent was monitored for its sorption profiles into the acrylic films, Avanse MV-100 (Figure 9) and Joncryl 74 (Figure 10), and the sorption characteristics observed were normalized against the saturation of water. In each acrylic film, after initial saturation by water, paraoxon was observed to accumulate/concentrate within the film independent of the aqueous medium (Figure 9 and 10).

The initial water saturation and challenge agents followed the diffusion profile of a two-step process (Figure 9 and 10). The equilibrium of water sorption into the acrylic films revealed that the challenge agent has a higher affinity for the polymer than water. The resulting curve was observed as a Fickian sorption profile that appeared after the initial saturation of water had been reached within Avanse MV-100 (Figure 9). Furthermore, sorption of the aqueous challenge agent paraoxon in Joncryl-74 subsequent to initial saturation of water indicated a non-Fickian sorption of paraoxon with an equal desorption of water within the same film (Figure 10). The data support a conclusion that the affinity of the acrylic dispersion and acrylic emulsion for the challenge agent allows for a solvation effect by the polymer to singularly increase the interior film concentration of the reactants beyond the water solvation capacity. However, the effect is slow, and was observed over elongated observations of the sorption profiles for the challenge agent paraoxon. The aqueous solvated demeton-S sorption profile into the acrylic films followed Fickian sorption profile for Avanse MV-100 (Figure 11), and non-Fickian sorption profile for Joncryl 74 (Figure 12). The sorption of aqueous demeton-S into Joncryl 74 was 3.56×10^{-10} cm^2 s^{-1}, which (as a reference point) was 280 times less than the calculated sorption rate of 9.97×10^{-8} cm^2 s^{-1} of aqueous demeton-S into Avanse MV-100.

The fourth polymer type, Hybridur 570/580 polyurethane dispersion, had a measured T-T_g of 56.1 ℃. The observed sorption profile of the two challenge agents into the rubbery solid film was Fickian (Figure 13 and 14), which followed the expected sorption profile for a rubbery film as described previously.[22,15,23]

The water saturated sorption profiles of the challenge agents were observed as near Fickian characteristics for the aqueous phase. However, it was observed that Hybridur 570/580 had differential solubility for water and each challenge agent singularly. Neither paraoxon nor demeton-S was observed at the film-substrate interface in the aqueous sorption profile, and suggests a differential sorption for the water saturated reactants that were exclusive for the aqueous phase of the challenge (Figures 15 and 16).

Self-Decontamination Activity for OPH versus Simulate Agent and Polymer Type

The activity of the embedded OPH was measured against the challenge agents as neat and aqueous solvated reactants. Neat paraoxon was placed on the film interface and monitored for hydrolysis by the embedded OPH. The biocatalyst activity was plotted in terms of mass in grams hydrolyzed per unit time as a function of surface area in square meters. The mass of neat challenge agent hydrolyzed was 7.8 $g/min/m^2$ in the Avanse MV-100 acrylic film for neat paraoxon (Figure 17) and 0.83 ± 0.12 $g/h/m^2$ for neat demeton-S (Figure 18). Neat paraoxon was hydrolyzed in Joncryl 74 at a rate of 7.9 ± 1.9 $g/min/m^2$, but only at 0.14 ± 0.03 $g/h/m^2$ when challenged by neat demeton-S (Figures 17 and 18).

Although both acrylic films had similar hydrolysis rates when challenged by neat paraoxon, there was an 83% loss in relative activity for the hydrolysis of neat demeton-S in Joncryl 74 relative to Avanse MV-100. The sorption characteristics for neat paraoxon for both acrylic films were similar and non-Fickian, which may explain the similarities in hydrolysis rates of paraoxon. The sorption profiles for neat demeton-S differed between Avanse MV-100 and Joncryl 74. Joncryl 74 had a pseudo-Fickian sorption profile for neat demeton-S (Figure 6); however, Avanse MV-100 displayed a two-step diffusion process

followed by a Fickian sorption profile that explains the greater hydrolysis rate in Avanse MV-100 over Joncryl 74 (Figure 8).

Hydrolysis of the aqueous solvated challenge agents in acrylic films was measured to determine the sorption dependent rate limited hydrolysis. The rate of hydrolysis for water carried paraoxon in Avanse MV-100 films was 5.4 ± 0.53 g/min/m^2 as compared to 3.4 ± 1.1 g/min/m^2 in Joncryl 74. The observed difference in sorption profiles between these two films for post-water saturated accumulation of paraoxon had a Fickian profile for Avanse MV-100 (Figure 9) and a sigmoidal profile for Joncryl 74 (Figure 10). The post-water saturation accumulation of paraoxon in Avanse MV-100 was independent of the observed water desorption rate, indicating that there may be some solvation of paraoxon in the polymer phase that is exclusive of the water phase and allows higher concentration of paraoxon at the catalytic site of the active OPH additive (Figure 9, inset). The post-water saturation rate of paraoxon accumulation was dependent on the water desorption rate in Joncryl 74, indicating that the accumulation of paraoxon in Joncryl 74 was dependent on water desorption in the aqueous phase. The rate of exchange between water and paraoxon within Joncryl 74 resulted in lower accumulation of paraoxon in the film for hydrolysis by the embedded OPH (Figure 10, Inset).

The enzyme activity observed in solid films was not limited by the binding affinity of the enzyme for the reactant (K_m), but by the diffusion rate of the reactant to the binding site of the active enzyme into the solid phase films and possibly by the diffusion of hydrolysis products away from the enzyme into the solid matrix. To describe the OPH hydrolysis activity embedded in films using aqueous solvated demeton-S, the rate of hydrolysis was plotted as a function of challenge concentration and found to follow classical enzyme kinetics saturation with apparent K_m values. Therefore, the reported apparent K_m values observed for this system are not the classical K_m values described for the binding affinity of the enzyme for the reactant and will be denoted by K_m^D to avoid confusion, which has been previously described by Halling to theoretically model diffusion of reactants in polymer films for immobilized enzymes.[24] Modeling the OPH activity based on the apparent K_m^D and V_{max} values for the different film types using equation 3 [24] allows for modeled comparison of reactant diffusion rates and enzyme activity retention of the embedded OPH additive.

$$v(A,P) = \frac{\left[\frac{V_{max}}{K_A}\left(A - \frac{P}{K}\right)\right]}{1 + \frac{A}{K_A} + \frac{P}{K_P}} \qquad \text{(Eq. 3)}^{24}$$

Where A is the reactant initial concentration, P is the initial product concentration, K_A and K_P are the Michaelis constants with units of moles per unit volume, K is the dimensionless equilibrium constant, and V_{max} is the Michaelis-Menten maximum forward velocity with dimensions of moles per unit time.

Evaluating the hydrolysis of aqueous solvated demeton-S by OPH in the four film types indicates that the OPH additive embedded in Avanse MV-100 film has the greatest calculated rate of hydrolysis at 2.8 ± 0.12 µ*M*/min with an apparent K_m^D value of 4.4 ± 0.34 m*M* demeton-S (Figure 19). The second highest OPH hydrolysis activity challenged with aqueous demeton-S was observed in Eponol with a calculated V_{max} of 1.1 ± 0.02 µ*M*/min and an apparent K_m^D of 8.25 ± 0.27 m*M* demeton-S (Figure 19). Within the error range of OPH additive activity, Joncryl 74 and Hybridur 570/580 had the least measurable activity of demeton-S hydrolysis. The calculated V_{max} of Hybridur 570/580 was 0.58 ± 0.05 µM/min and 0.44 µ*M*/min for Joncryl 74 (Figure 19). The error calculation in the apparent K_m^D for both Joncryl 74 and Hybridur 570/580 are too great to provide a reliable K_m^D estimation because of the low or nonexistent sorption of aqueous demeton-S into the films, and was consistent with the observed differential diffusion of aqueous demeton-S into Hybridur 570/580 (Figure 16).

The hydrolysis rate observed in the linear thermoplastic epoxy (Eponol) film was measured as challenged with neat paraoxon and neat demeton-S. The OPH hydrolysis activity observed from challenging by neat paraoxon was 1.5 ± 0.45 g/min/m^2 (Figure 17) and neat demeton-S was 0.66 ± 0.19 g/h/m^2 (Figure 18). Relative to OPH hydrolysis activity embedded in Avanse MV-100 film (for normalization), the catalytic difference was 81% less for the hydrolysis of paraoxon, and 20% less for the hydrolysis of neat demeton-S. The sorption of neat paraoxon into Eponol was observed to be a two-step process (Figure 1) and the sorption of demeton-S was observed to be Fickian (Figure 2). Although the two films appear to have similar initial rates of sorption with demeton-S having a slightly higher diffusion

rate, the difference in hydrolysis rate was 61% in favor of demeton-S as compared to the observed maximum in Avanse MV-100. Monitoring the activity profile in neat demeton-S with increasing OPH incorporation revealed that at 3% additive incorporation in Eponol, the hydrolysis of demeton-S becomes non-linear compared with the other film types (Figure 20). At the measured hydrolysis rate of neat paraoxon, the two-step process for diffusion would indicate that paraoxon first fills the available void space in the films followed by a sorption rate of the reactant that is dependent on the affinity of the polymer for sorbent in a process described previously by Philippe and coworkers.[15,22] In comparison with the sorption of demeton-S into Eponol, the Fickian profile indicates a single step diffusion that quickly and evenly diffuses the reactant into the film, and may explain the increase in hydrolysis rate by OPH against neat demeton-S as compared to paraoxon.

The hydrolysis rate of aqueous solvated paraoxon in Eponol was measured to be 0.16 ± 0.11 g/min/m^2 (Figure 18), i.e., a loss in hydrolysis activity of 97% in Eponol for aqueous paraoxon as normalized against Avanse MV-100. The sorption of aqueous paraoxon into Eponol was observed to be pseudo-Fickian with a diffusion rate of 1.62 x 10^{-9} cm^2 s^{-1} and a dependant sorption with the water phase at the same rate (Figure 3). The observation indicates that paraoxon and water diffuse into the film at the same rate and that the polymer phase does not accumulate paraoxon differentially from water as observed in the acrylic films Avanse MV-100 (Figure 9) and Joncryl 74 (Figure 10). The observed slower sorption of aqueous paraoxon into Eponol correlates with the low measured OPH hydrolysis activity in film, and supports the hypothesis that the activity of the embedded OPH additive is partially dependent on the sorption of the reactant to the catalytic site on the active enzyme.

The hydrolysis rate of neat paraoxon in Hybridur 570/580 polyurethane dispersion film by the embedded OPH additive was measured to be 0.43 ± 0.20 g/min/m^2, i.e., a loss in OPH hydrolysis activity of 95% activity compared with the OPH activity in Avanse MV-100 film (Figure 17). The hydrolysis of neat demeton-S was measured to be 0.006 ± 0.001 g/h/m^2, i.e., a loss in activity of 99% compared with the OPH activity in Avanse MV-100 film (Figure 18). The diffusion of neat paraoxon (Figure 13) and demeton-S (Figure 14) followed a non-Fickian sigmoidal sorption profile at1.42 x 10^{-9} cm^2 s^{-1} and 1.15 x 10^{-8} cm^2 s^{-1}, respectively. The low sorption of the reactants into the films resulted in low accumulation of reactants at the catalytic site of the active OPH additive. Unlike the aqueous solvated reactants, a sorption profile was not observed for either paraoxon or demeton-S. The embedded OPH additive hydrolysis activity against the aqueous solvated challenge agents was measured as zero for aqueous paraoxon (Figure 21) and a near zero conversion rate of 0.0003 ± 0.0 g/h/m^2 for aqueous demeton-S (Figure 19). The low diffusion rate coupled with the low OPH hydrolysis rate in Hybridur 570/580 supports the hypothesis that reactant diffusion into the polymer phase to the catalytic site on the active embedded biocatalyst is essential for synergistic engineering of the polymer phase with the substrate selected for the challenge agent.

Discussion

The research objective was to investigate the possibility that the selection of diffusing reactants affects the catalytic rate of the embedded enzymatic additives within solid films. Several studies have investigated enzyme activity retention in solid matrix as a function of embedding the biomaterial into a solid support. Furthermore, the enzyme activity retained within a solid matrix material has been shown to depend on the enzyme's conformation, orientation, and physical state after incorporation.[25-32] As importantly, it was suggested that after enzyme modification to stabilize the three dimensional protein structures to retain activity, the loss in solid state catalysis was due to enzyme deformation.[32-34,35-39] Using kinetic profiles related to matrix-free catalytic additives, Tong and coworkers demonstrated loss of enzyme activity due to denaturation of the active site. However, the reactants (substrates) used in these studies were not investigated for their sorption within the solid matrix material.[32] The data presented here suggest previously reported data purportedly showing loss in activity due to denaturation is an overestimation because the reactants may not have been allowed time to diffuse or may not have diffused to the catalytic site of the active enzymes on a time scale adequate for characterization.[33]

Functional films are interesting and require understanding to properly engineer coatings that incorporate latent and specific catalytic functions in the bulk phase. Property and performance optimization of the selected polymer type must match the sorption characteristics of the reactants (in our case chemical warfare agent simulants, though very generally applicable to a wide range of potential

functional enzymatic additive/enzymatic substrate pairs) that challenge the solid phase reactors must be characterized and understood. The enzyme activity retained in the solid phase should be characterized dependent on the sorption of the reactants into the solid matrix. Reactant sorption should be monitored as a means for proper polymer type selection to match necessary decontamination activity with environmental specificity, e.g., low or high humidity in light of the potential for a "filtering" effect for water delivered agents. Without understanding reactant sorption into the solid matrix, the retained enzyme activity characterization methodologies are liable to mischaracterize the latent functionality, activity, and retention/optimization of the functional coating. Previously reported activity of embedded enzymes in a waterborne polyurethane coating suggested that the sorption of the reactant into the bulk phase of the coating by first saturating the coating in an aqueous buffer was sufficient for characterization of embedded biocatalysts activity retention.[33] However, the rate of sorption reported by saturating the waterborne polyurethane in buffer resulted in a possible twenty-fold reduction in effective reactant concentration for the bulk phase saturation of the embedded enzyme for the analysis period reported. Coating characterization based on the catalytic rate of the embedded enzyme as a function of activity retention based on the embedding process underestimates the functional retention of the enzymes based on the loss of reactant sorption to the functional site of the active enzyme by as much as 63%.[33] Without characterizing the sorption of the reactant independent of an aqueous phase, the activity retention of the embedded biocatalyst in solid polymer coatings may be misrepresented. It is likely that the previously reported percent activity retention of embedded enzymes in waterborne polyurethane coatings is greater than calculated values for the assay period investigated.[33]

The uptake of the reactants into the polymer phase shown here supports the need for selecting the polymer to closely match the solubility parameters of the penetrant for optimal functionality. The observed solubility of the reactants by the polymer in correlation with the measured activity demonstrates that the uptake and diffusion of the reactant was the rate limiting step for this system. Closely aligning the Hansen solubility parameter of the reactant with that of the polymer will result in optimal efficiency of the immobilized biocatalyst by ensuring a reduction in diffusional constraints and enable saturation of the enzyme active site.

Summary

To optimize the activity of embedded biocatalysts, judicial selection of the solid phase polymer type is as important as the embedded functional additive. Sorption of the simulant challenge agents to the functional site on the active biocatalysts is the rate limiting factor for solid phase catalysis. Engineering functional coatings with latent, stable, extended film-life catalytic capabilities requires foreknowledge of the functional challenge and dependency on the environmental conditions for certain polymer and challenge agent combinations. Characterizing the activity retention of the embedded biocatalyst with the sorption rate of the challenge agent that saturates the catalytic site of the additive will allow for a more complete understanding of the utility for functional coating systems. Rapid grafting of the wide number of available bio-based catalytic activities into polymer systems will require such an understanding in order to bring laboratory results into a commercial product in the shortest time.

References

(1) Zaks, A.; Klibanov, A. M. *Science (Washington, DC, United States)* **1984**, *224*, 1249.
(2) Zaks, A.; Klibanov, A. M. *Proceedings of the National Academy of Sciences of the United States of America* **1985**, *82*, 3192.
(3) Laane, C.; Boeren, S.; Vos, K.; Veeger, C. *Biotechnol Bioeng* **1987**, *30*, 81.
(4) Cao, L.; Langen, L. v.; Sheldon, R. A. *Current Opinion in Biotechnology* **2003**, *14*, 387.
(5) Chaplin, M. F.; Bucke, C. *Enzyme technology*; Cambridge University Press: Cambridge, England, 1990; Vol. xvi.
(6) Goddard, J. M.; Hotchkiss, J. H. *Progress in Polymer Science* **2007**, *32*, 698.
(7) Pierre, A. C. *Biocatalysis and Biotransformation* **2004**, *22*, 145.
(8) Barton, A. F. M. *CRC handbook of solubility parameters and other cohesion parameters*; CRC Press: Boca Raton, Fla., 1983.
(9) Novick, S. J.; Dordick, J. S. *Biotechnology and Bioengineering* **2000**, *68*, 665.

(10) Chen, B.; Miller, E. M.; Miller, L.; Maikner, J. J.; Gross, R. A. *Langmuir* **2006**, *23*, 1381.
(11) McDaniel, C. S.; McDaniel, J.; Wales, M. E.; Wild, J. R. *Prog. Org. Coat.* **2006**, *55*, 182.
(12) Rawlins, J. W.; Wales, M. E. *European Coatings Journal* **2008**, 26.
(13) Karlsson, O. J.; Stubbs, J. M.; Karlsson, L. E.; Sundberg, D. C. *Polymer* **2001**, *42*, 4915.
(14) Talbot, A.; Kitchener, J. A. *British Journal of Applied Physics* **1956**, *7*, 96.
(15) Philippe, L.; Sammon, C.; Lyon, S. B.; Yarwood, J. *Progress in Organic Coatings* **2004**, *49*, 315.
(16) Crank, J. *The Mathematics of Diffusion*; 2 ed.; Oxford University Press, 1979.
(17) Park, G. S. *Diffusion in polymers*; Academic Press: New York, 1968; Vol. xii.
(18) Bagley, E.; Long, F. A. *Journal of the American Chemical Society* **1955**, *77*, 2172.
(19) Rogers, C. E. *Physics and Chemistry of the Organic Solid State*; Wiley-Interscience: New York, 1965; Vol. 2.
(20) Newns, A. C. *Transactions of the Faraday Society* **1956**, *52*, 1533.
(21) Flory, P. J. *Principles of polymer chemistry*; Cornell University Press: Ithaca, 1953.
(22) Philippe, L.; Sammon, C.; Lyon, S. B.; Yarwood, J. *Progress in Organic Coatings* **2004**, *49*, 302.
(23) M. Le Meste, D. C., G. Roudaut, G. Blond, D. Simatos *Journal of Food Science* **2002**, *67*, 2444.
(24) Halling, P. J.; Wilson, S. K.; Jacobs, R.; McKee, S.; Coles, C. W. *Biotechnology Progress* **2003**, *19*, 1228.
(25) Gill, I.; Ballesteros, A. *Trends Biotechnol* **2000**, *18*, 469.
(26) Novick, S. J.; Dordick, J. S. *Biomaterials* **2002**, *23*, 441.
(27) Kim, Y. D.; Dordick, J. S.; Clark, D. S. *Biotechnology and Bioengineering* **2001**, *72*, 475.
(28) Lei, C. H.; Shin, Y. S.; Liu, J.; Ackerman, E. J. *Journal of the American Chemical Society* **2002**, *124*, 11242.
(29) Drott, J.; Lindstroem, K.; Rosengren, L.; Laurell, T. *Journal of Micromechanics and Microengineering* **1997**, *7*, 14.
(30) Avnir, D.; Braun, S.; Lev, O.; Ottolenghi, M. *Chemistry of Materials* **1994**, *6*, 1605.
(31) Gill, I.; Ballesteros, A. *Journal of the American Chemical Society* **1998**, *120*, 8587.
(32) Tong, X.; Trivedi, A.; Jia, H.; Zhang, M.; Wang, P. *Biotechnology Progress* **2008**, *24*, 714.
(33) Russell, A. J.; Erbeldinger, M.; DeFrank, J. J.; Kaar, J.; Drevon, G. *Biotechnology and Bioengineering* **2002**, *77*, 352.
(34) Clark, D. S. *Trends Biotechnol* **1994**, *12*, 439.
(35) Cabral, J. M. S.; Kennedy, J. F. *Thermostab. Enzymes* **1993**, 162.
(36) Rocchietti, S.; Urrutia, A. S. V.; Pregnolato, M.; Tagliani, A.; Guisan, J. M.; Fernandez-Lafuente, R.; Terreni, M. *Enzyme and Microbial Technology* **2002**, *31*, 88.
(37) Tischer, W.; Kasche, V. *Trends Biotechnol.* **1999**, *17*, 326.
(38) Tischer, W.; Wedekind, F. *Topics in Current Chemistry* **1999**, *200*, 95.
(39) Janssen, M. H. A.; Van Langen, L. M.; Pereira, S. R. M.; Van Rantwijk, F.; Sheldon, R. A. *Biotechnology and Bioengineering* **2002**, *78*, 425.

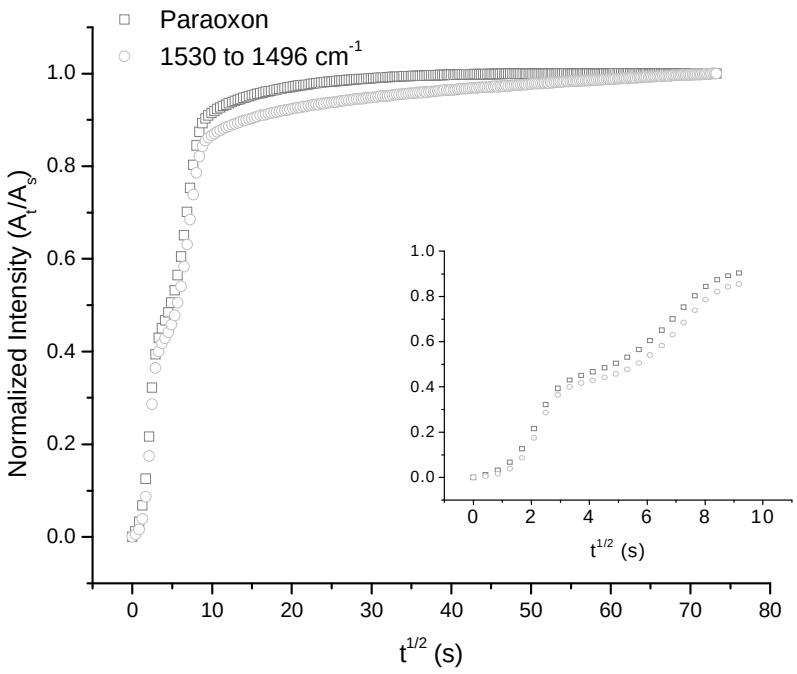

Figure 1: Neat paraoxon sorption into an Eponol 53-BH-35 epoxy film. Component sorption plot of neat paraoxon monitored at the substrate-film interface for Eponol 53-BH-35 film as observed by IR fingerprint using ATR-IR analysis software. Aromatic C=C stretch between 1530 and 1496 cm^{-1} trace plotted as validation control for subsequent aqueous solvated sorption monitoring.

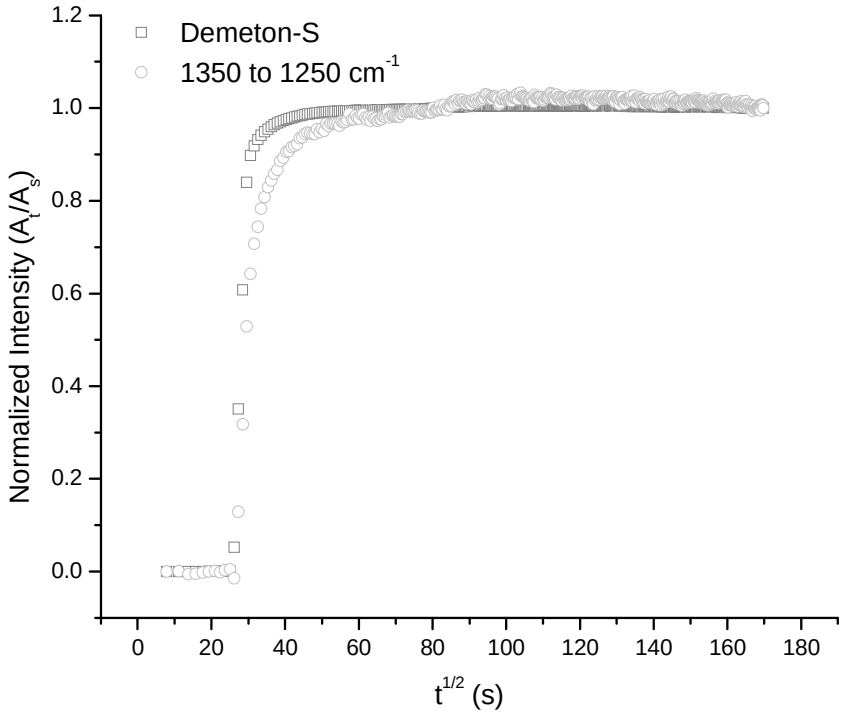

Figure 2: Neat demeton-S sorption into an Eponol 53-BH-35 epoxy film. Component sorption plot of neat demeton-S monitored at the substrate-film interface for Eponol 53-BH-35 film as observed by IR fingerprint using ATR-IR analysis software. Phosphoryl stretch between 1350 and 1250 cm^{-1} trace plotted as validation control for subsequent aqueous solvated sorption monitoring.

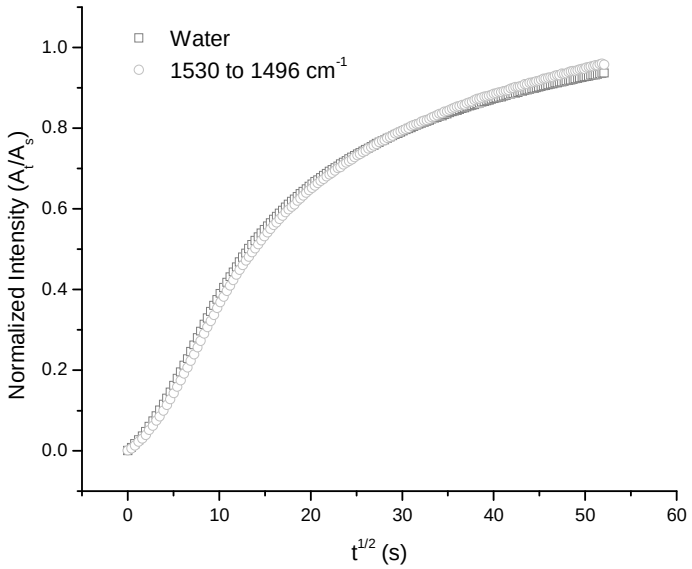

Figure 3: Aqueous paraoxon sorption into an Eponol film. Sorption profile of water saturated paraoxon at 1530 to 1496 cm^{-1} normalized against sorption profile of water into Eponol 53-BH-35 film as observed at the substrate-film interface.

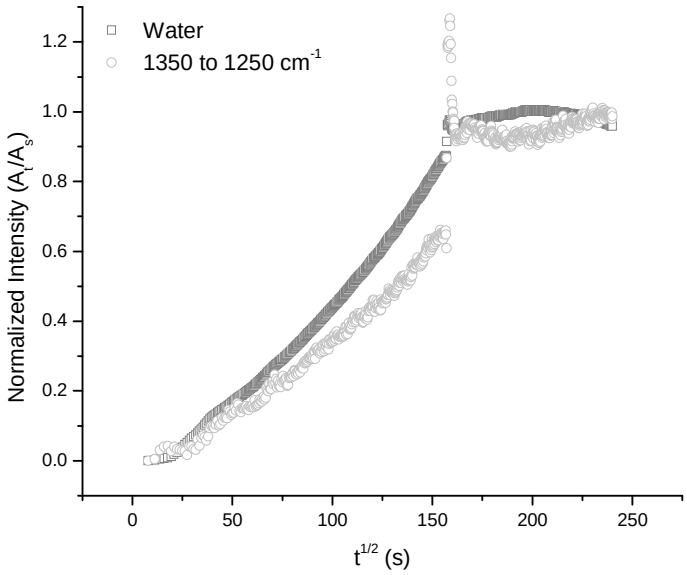

Figure 4: Aqueous demeton-S sorption into Eponol film. Sorption profile of water saturated demeton-S at 1350 to 1250 cm^{-1} normalized against sorption profile of water into Eponol 53-BH-35 film as observed at the substrate-film interface.

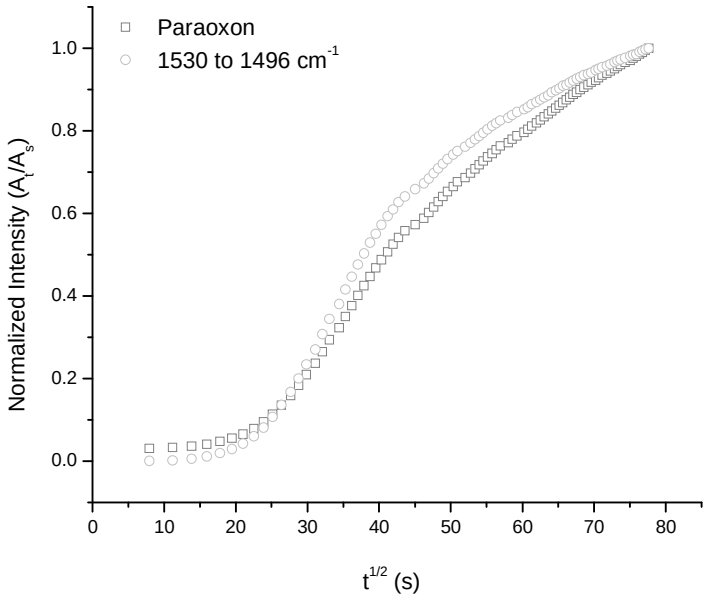

Figure 5: Neat paraoxon sorption into a Joncryl 74 film. Component sorption plot of neat paraoxon monitored at the substrate-film interface for Joncryl 74 film as observed by IR fingerprint using ATR-IR analysis software. Aromatic C=C stretch between 1530 and 1496 cm^{-1} trace plotted as validation control for subsequent aqueous solvated sorption monitoring.

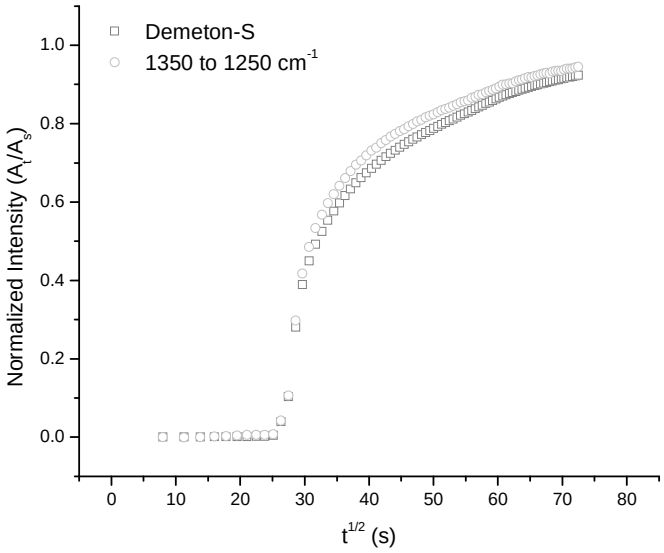

Figure 6: Neat demeton-S sorption into a Joncryl 74 film. Component sorption plot of neat demeton-S monitored at the substrate-film interface for Joncryl 74 film as observed by IR fingerprint using ATR-IR analysis software. Phosphoryl stretch between 1350 and 1250 cm^{-1} trace plotted as validation control for subsequent aqueous solvated sorption monitoring.

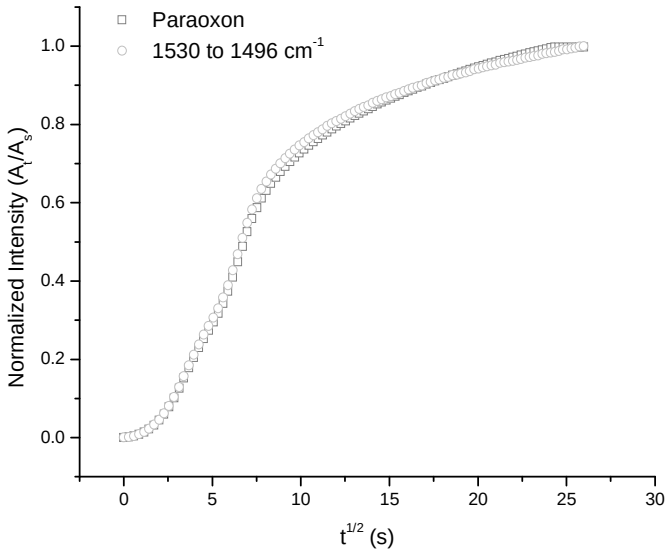

Figure 7: Neat paraoxon sorption into an Avanse MV-100 film. Component sorption plot of neat paraoxon monitored at the substrate-film interface for Avanse MV-100 film as observed by IR fingerprint using ATR-IR analysis software. Aromatic C=C stretch between 1530 and 1496 cm^{-1} trace plotted as validation control for subsequent aqueous solvated sorption monitoring.

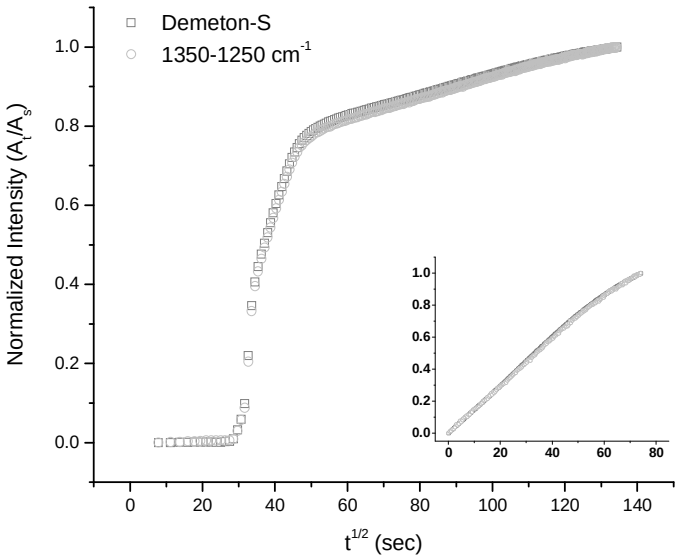

Figure 8: Sorption of neat demeton-S into an Avanse MV-100 film. Component sorption plot of neat demeton-S monitored at the substrate-film interface for Avanse MV-100 film as observed by IR fingerprint using ATR-IR analysis software. Phosphoryl stretch between 1350 and 1250 cm^{-1} trace plotted as validation control for subsequent aqueous solvated sorption monitoring. Fickian second step sorption plotted in inset from point of inflection after step one sorption.

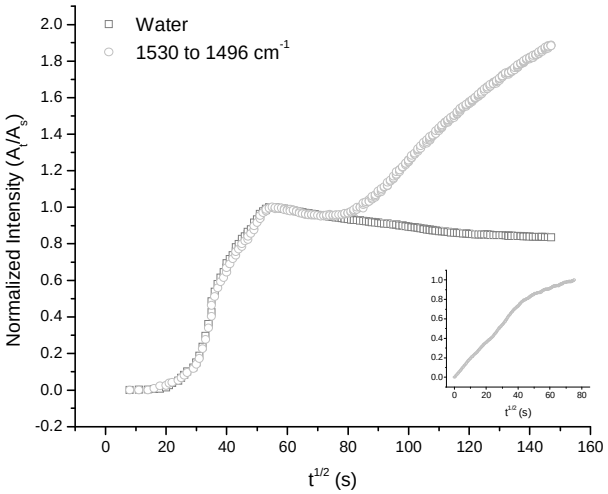

Figure 9: Aqueous paraoxon sorption profile into an Avanse MV-100 film. Sorption profile of water saturated paraoxon at 1530 to 1496 cm^{-1} normalized against sorption profile of water into Avanse MV-100 film as observed at the substrate-film interface. The sorption profile of water followed a characteristic two-step diffusion process. Post-equilibrium sorption of paraoxon observed after water saturation was observed as a deviation from the sorption curve of water. Inset is paraoxon sorption into Avanse MV-100 after equilibrium has been established for water. Sorption profile for paraoxon after water equilibrium indicates Fickian sorption characteristics.

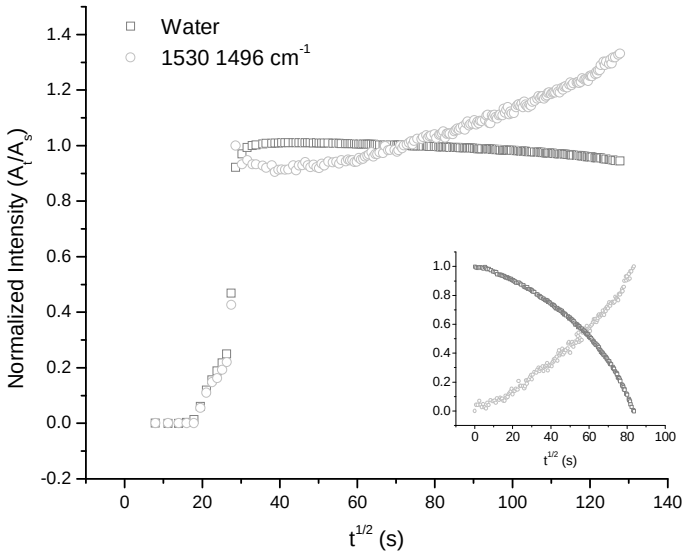

Figure 10: Aqueous paraoxon sorption into a Joncryl 74 film. Sorption profile of water saturated paraoxon normalized against sorption profile of water into Joncryl-74. Water sorption profile into Joncryl-74 indicated a characteristic two-step diffusion process. Continued sorption of paraoxon observed after water saturation was observed as a deviation from the sorption curve of water. Inset is paraoxon sorption and water desorption in Joncryl-74 after initial saturation has been established for water. Sorption profile for paraoxon after initial water saturation indicated non-Fickian sorption characteristics.

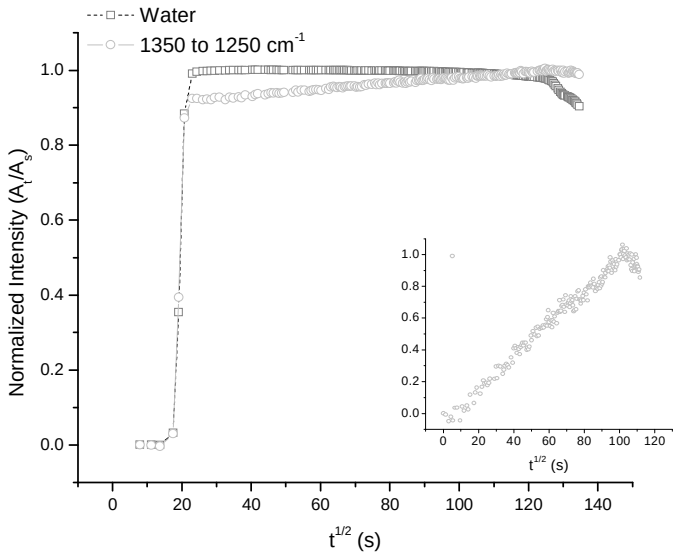

Figure 11: Aqueous demeton-S sorption into an Avanse MV-100 film. Sorption profile of water saturated demeton-S at 1350 to 1250 cm^{-1} normalized against sorption profile of water into Avanse MV-100 film as observed at the substrate-film interface. Inset is demeton-S sorption into Avanse MV-100 after equilibrium has been established for water. Sorption profile for demeton-S after water equilibrium indicates Fickian sorption characteristics.

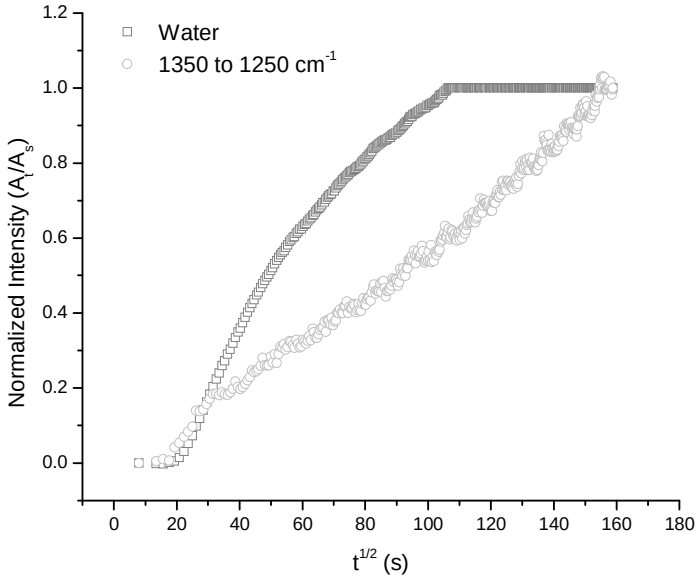

Figure 12: Aqueous demeton-S sorption into a Joncryl 74 film. Sorption profile of water saturated demeton-S at 1350 to 1250 cm^{-1} normalized against sorption profile of water into Joncryl 74 film as observed at the substrate-film interface.

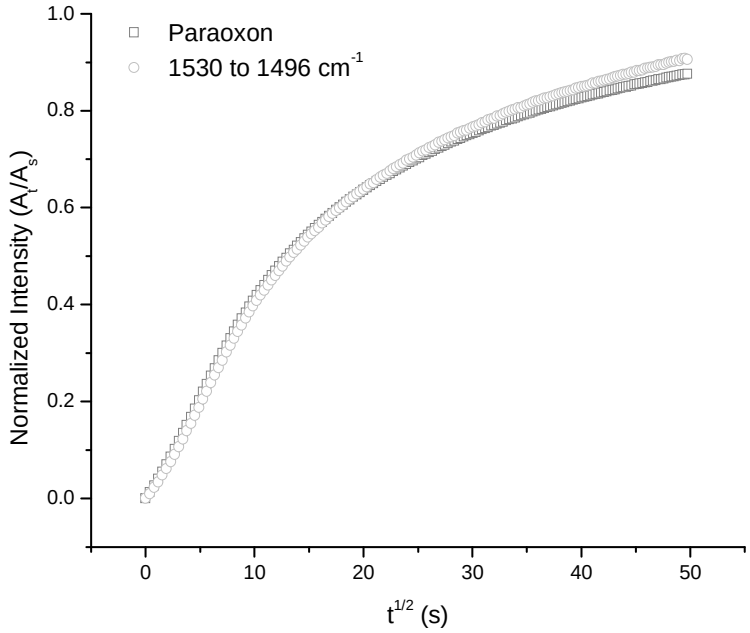

Figure 13: Neat paraoxon sorption into a Hybridur 570/580 polyurethane film. Component sorption plot of neat paraoxon monitored at the substrate-film interface for Hybridur 570/580 film as observed by IR fingerprint using ATR-IR analysis software. Aromatic C=C stretch between 1530 and 1496 cm^{-1} trace plotted as validation control for subsequent aqueous solvated sorption monitoring.

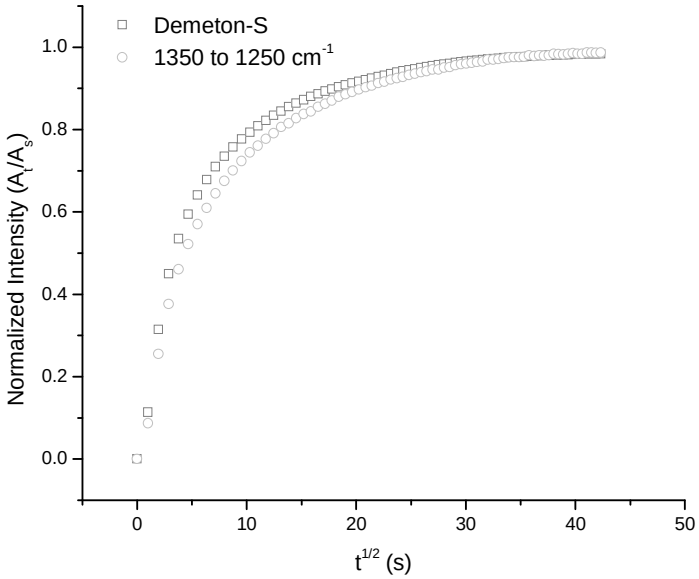

Figure 14: Neat demeton-S sorption into a Hybridur 570/580 polyurethane film. Component sorption plot of neat demeton-S monitored at the substrate-film interface for Hybridur 570/580 film as observed by IR fingerprint using ATR-IR analysis software. Phosphoryl stretch between 1350 and 1250 cm^{-1} trace plotted as validation control for subsequent aqueous solvated sorption monitoring.

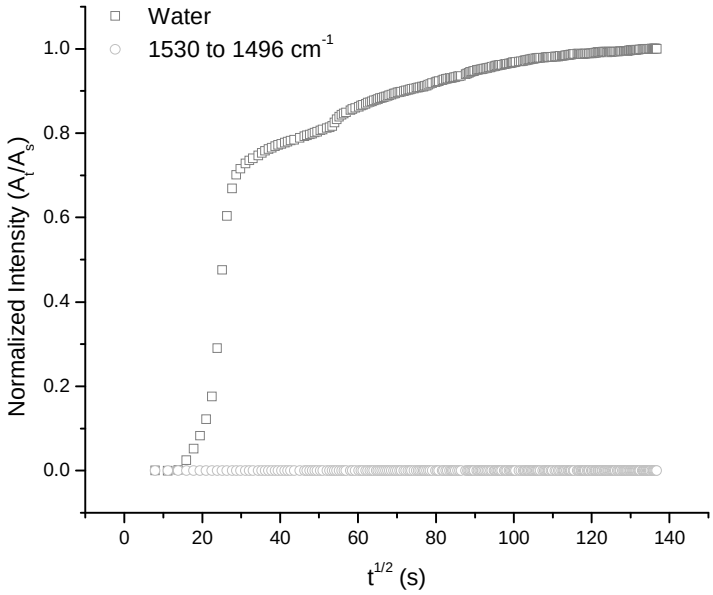

Figure 15: Aqueous paraoxon sorption into a Hybridur 570/580 polyurethane film. Sorption profile of water saturated paraoxon at 1530 to 1496 cm^{-1} normalized against sorption profile of water into Hybridur 570/580 film as observed at the substrate-film interface.

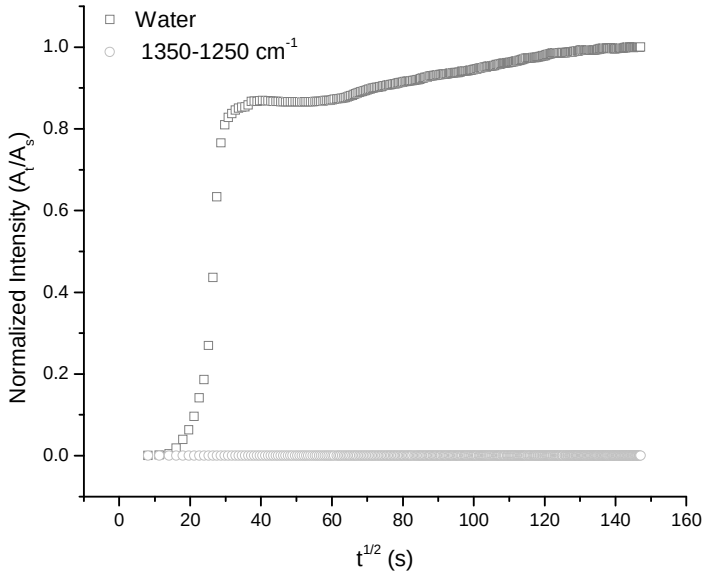

Figure 16: Aqueous demeton-S sorption into a Hybridur 570/580 polyurethane film. Sorption profile of water saturated demeton-S at 1350 to 1250 cm^{-1} normalized against sorption profile of water into Hybridur 570/580 film as observed at the substrate-film interface.

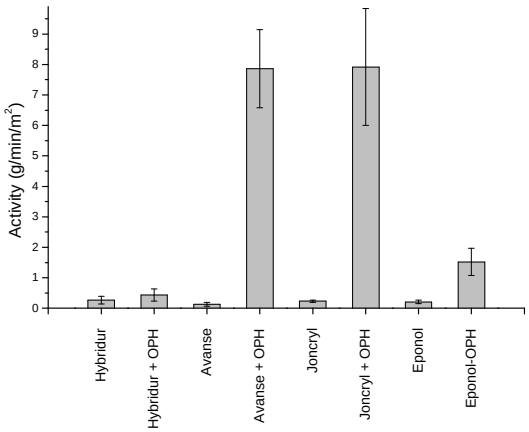

Figure 17: Activity of the embedded OPH additive challenged against neat paraoxon monitored at 405 nm.

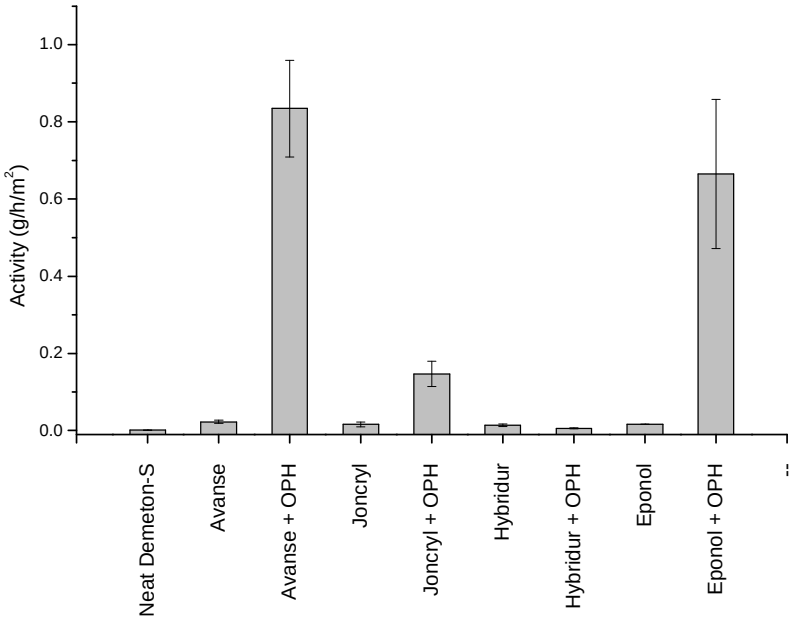

Figure 18: Activity of the embedded OPH additive challenged against neat demeton-S as observed at 405 nm.

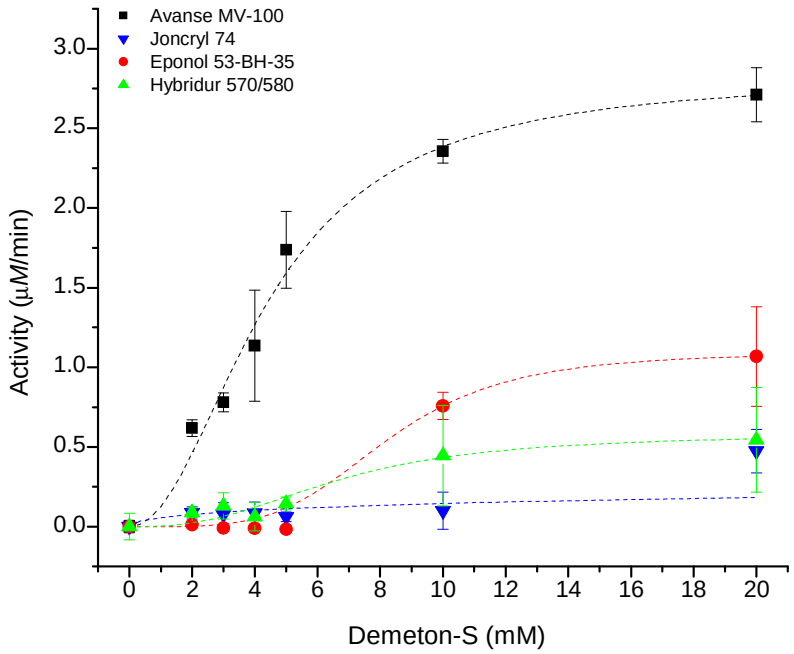

Figure 19: Diffusion-based kinetic analysis for embedded OPH additive in coating films challenged with aqueous solvated demeton-S. Curve fitting was accomplished by modeling sigmoidal fit as indicated by the dotted lines. Curve modeling method was similar to K_m curve fit method for free protein in solution using Michaelis-Menten modeling. The K_m apparent values obtained are not considered true K_m values, but reactant concentrations that have reached maximum sorption into solid material to the active site of stable enzymes (K_m^D). R^2 curve fit for Avanse MV-100 was 0.9880, for Eponol 0.9999, for Hybridur 570/580 0.9683, and 0.09727 for Joncryl 74.

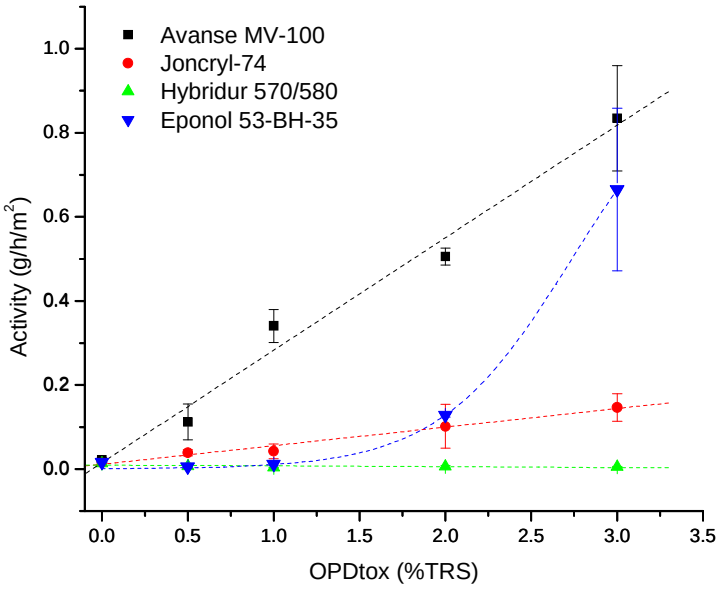

Figure 20: Activity profile of embedded OPH additive challenged against neat demeton-S as observed at 405 nm. Curve fitting indicated as dotted lines are linear for Avanse MV-100, Hybridur 570/580, and Joncryl 74. Eponol activity was modeled as sigmoidal as indicated by the non-linear blue dotted line.

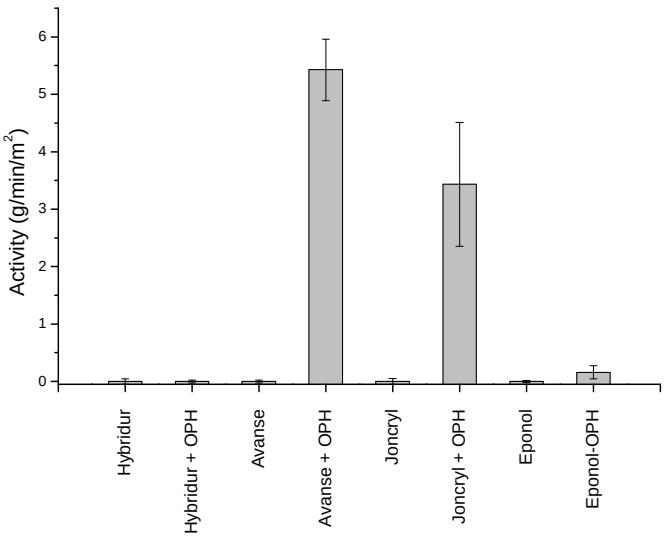

Figure 21: Measured activity of film samples with embedded OPH hydrolase challenged against aqueous paraoxon monitored at 405 nm.

Table 1: Kinetics of sorption of H_2O, demeton-S or paraoxon into polymer films Avanse MV-100, Joncryl 74, Eponol 53-BH-35, and Hybridur 570/580.

Polymer type / Penetrant	ATR-IR	*Diffusion Coefficient D (cm^2 s^{-1})* Initial Sorption	Secondary Sorption
Avanse MV-100 / demeton-S	demeton-S	2.56E-08	9.68E-11
	1350-1250 cm^{-1}	2.51E-08	8.54E-11
	H_2O	1.01E-06	1.94E-13
	1350-1250 cm^{-1}	9.97E-08	8.79E-12
Avanse MV-100 / paraoxon	paraoxon	3.61E-08	
	1530 to 1496 cm^{-1}	3.62E-08	
	H_2O	1.80E-08	3.53E-11
	1530 to 1496 cm^{-1}	1.82E-08	3.14E-09
Joncryl 74 / demeton-S	demeton-S	5.50E-10	
	1350-1250 cm^{-1}	4.92E-10	
	H_2O	9.17E-10	
	1350-1250 cm^{-1}	3.56E-10	
Joncryl 74 / paraoxon	paraoxon	1.92E-08	
	1530 to 1496 cm^{-1}	2.34E-08	
	H_2O	4.46E-08	
	1530 to 1496 cm^{-1}	4.50E-08	
Eponol 53-BH-35 / demeton-S	demeton-S	6.04E-08	
	1350-1250 cm^{-1}	5.94E-08	
	H_2O	4.09E-10	
	1350-1250 cm^{-1}	2.25E-10	
Eponol 53-BH-35 / paraoxon	paraoxon	1.16E-08	
	1530 to 1496 cm^{-1}	9.77E-09	
	H_2O	1.64E-09	
	1530 to 1496 cm^{-1}	1.62E-09	
Hybridur 570/580 / demeton-S	demeton-S	1.15E-08	
	1350-1250 cm^{-1}	8.56E-09	
	H_2O	1.70E-08	
	1350-1250 cm^{-1}	0.00E+00	
Hybridur 570/580 / paraoxon	paraoxon	1.43E-09	
	1530 to 1496 cm^{-1}	1.42E-09	
	H_2O	1.32E-08	
	1530 to 1496 cm^{-1}	0.00E+00	